J|A|C|S
ARTICLES
Published on Web 06/16/2006

Experimental and Theoretical Electron Density Study of Estrone

Elizabeth A. Zhurova,[†] Chérif F. Matta,[‡] Nan Wu,[†,§] Vladimir V. Zhurov,[†] and A. Alan Pinkerton*[,†]

Contribution from the Department of Chemistry, University of Toledo, Toledo, Ohio 43606, Department of Chemistry, Dalhousie University, Halifax, Nova Scotia, Canada B3H 4J3, and Department of Biochemistry, Case Western Reserve University, Cleveland, Ohio 44106

Received February 14, 2006; E-mail: apinker@uoft02.utoledo.edu

Abstract: The electron density and the electrostatic potential (ESP) distributions of estrone have been determined using X-ray diffraction analysis and compared with theoretical calculations in the solid and gas phases. X-ray diffraction measurements are performed with a Rigaku Rapid rotating anode diffractometer at 20 K. The electron density in the estrone crystal has been described with the multipole model, which allowed extensive topological analysis and calculation of the ESP. From DFT calculations in the solid state a theoretical X-ray diffraction data set has been produced and treated in the same way as the experimental data. Two sets of single molecule DFT calculations were performed: (a) An electron density distribution was obtained via a single-point calculation with a large basis set at the experimental geometry and subsequently analyzed according to the quantum theory of atoms in molecules (AIM) to obtain the bond and most atomic properties, and (b) another electron density distribution was obtained with a smaller basis set, but at a geometry optimized using the same basis set for the analysis of atomic energies. An interesting locally stabilizing hydrogen−hydrogen bond path linking H(1) and H(11B) is found which represents the first characterization of such bonding in a steroid molecule. AIM delocalization indices were shown to be well correlated to the experimental electron density at the bond critical points through an exponential relationship. The aromaticity of ring A, chemical bonding, the O(1)···O(2) distance necessary for estrogenic activity, and the electrostatic potential features are also discussed.

Introduction

Estrogens are known to be responsible for the development of secondary sexual characteristics, as well as effecting growth, differentiation, and function of a wide range of tissues. They have been extensively investigated since the role of estradiol in promoting breast cancer was determined.[1,2] Estrogens and related compounds bind as ligands to the estrogen receptor (ER) forming an activated complex. A series of events are initiated by the ER complex resulting in the activation or repression of selective genes and subsequent induction or suppression of the production of characteristic proteins. To better understand the role of the ligand in ER-mediated processes, extensive research into the influence of different estrogen derivatives on the regulation of hormone responsive genes has been carried out (see, for example, refs 2−8). Even though most changes in the estrogen ligand affect its affinity for the receptor, this does not necessarily correlate with the ligand's ability to stimulate the transcription of estrogen responsive genes. The mechanism by which these structurally altered ligands regulate the differential induction of gene expression is currently unknown. However, it has been suggested that the differences in the electrostatic potential generated by the lone pair electrons of the phenolic oxygen and π-electrons of the aromatic ring can be responsible for the variation in the regulation of hormone dependent genes.[6] It is obvious that the binding ability of the ligand to the receptor is not the only important factor in the biological activity of an estrogen or of a potential drug; secondary interactions and several domains of the receptor are involved. However, the initial driving force toward binding to a receptor must be due to the match between the topography of the electrostatic potential (ESP) of the estrogen or of a pharmacologically active molecule and that of the binding site.

Here we present a detailed electron density and electrostatic potential study of a natural estrogen, Estrone (3-hydroxy-1,3,5-(10)-estratrien-17-one):

[†] University of Toledo.
[‡] Dalhousie University.
[§] Case Western Reserve University.

(1) Wakeling, A. E.; Bowler, J. *J. Endocrinol.* **1987**, *112*, R7−R10.
(2) Parl F. F. *Estrogens, Estrone Receptor and Breast Cancer*. Amsterdam: IOS Press: 2000.
(3) Davis, M. D.; Butler, W. B.; Brooks, S. C. *J. Steroid Biochem. Mol. Biol.* **1995**, *52*, 421−430.
(4) Vander Kuur, J. A.; Wiese, T.; Brooks, S. C., *Biochemistry* **1993**, *32*, 7002−7008.
(5) Pilat, M. J.; Hafner, M. S.; Kral, L. G.; Brooks, S. C. *Biochemistry* **1993**, *32*, 7009−7015.
(6) Vander Kuur, J. A.; Hafner, M. S.; Christman, J. K.; Brooks, S. C. *Biochemistry* **1993**, *32*, 7016−7021.
(7) Adams, J.; Garcia, M.; Rochefort, H. *Cancer Res.* **1981**, *41*, 4720−4726.
(8) Brueggemeier, R. W.; Miller, D. D.; Dalton, J. T. In *Foye's Principles of Medicinal Chemistry*, 5th ed.; Williams, D.A., Lemke, T. L., Eds.; Lippincott Williams and Wilkins: Philadelphia, PA, 2002; pp 685−717.

10.1021/ja061080v CCC: $33.50

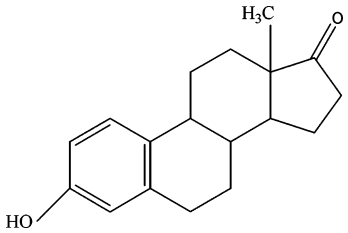

The estrone crystal exists in three different forms depending on the crystallization method.[9] We have performed both experimental and theoretical studies on form II (orthorhombic) of this crystal which can be easily crystallized, to give a better description of the properties of the compound as a whole, as well as its functional groups.

Experimental and Computational Details

A regularly shaped crystal (Table 1), crystallized from an ethanol/ethyl acetate solvent system, was mounted on the top of a glass capillary and slowly cooled to 20 K. The X-ray diffraction measurements were performed with a Rigaku R-Axis Rapid diffractometer with a high power Mo rotating anode generator (18 kW), graphite monochromator, and a curved image plate detector, with cooling provided by an open flow helium cryostat.[10−12] Low temperature significantly increased the atomic scattering power in the high angle area, and relatively strong spots were observed even at the edge of the detector at $2\theta \sim 140°$. To obtain high redundancy of data, six runs covering 0°−180° in ω were collected at different χ and φ settings, two at $\chi = 0°$ ($\varphi = 0°$, 180°) and four at $\chi = 45°$ ($\varphi = 90°$, 180°, 270°, 0°). The last run with $\varphi = 0°$ and $\chi = 45°$ was then eliminated due to temperature instability. For the first five runs the temperature varied by no more than 2°. To avoid significant overlap of reflections in any one image, a 4° ω-scan range was chosen. Oscillation ranges for adjacent images overlapped by 2° to provide precise scaling between them. Thus, each run consisted of a total of 89 images. An exposure time of 150 s per image was chosen to maximize scattering power and avoid saturation of the strongest reflections. The measurement was completed in ~44 h.

The collected data were indexed with the program *HKL2000*,[13] and the predicted reflection positions were used for data integration with the program *VIIPP*.[14,15] Oval integration boxes oriented along radial directions with variable size depending on the $\alpha_1-\alpha_2$ splitting were used. Since ~13% of the Bragg reflections from the estrone crystal have very low intensities (and were essentially unobserved), reflections below $4\sigma(I)$ were rejected during the integration, as well as partial and overlapped reflections. Data have been corrected for the floodfield distribution and the Lorentz-polarization effect. We considered the effects of absorption ($\mu = 0.08$ mm^{-1}) and thermal diffuse scattering at 20 K to be negligible. Data were scaled and then averaged in the 222 point group with the program *SORTAV*.[16] Most of the scaling factors for different images in the same run were very close to unity (usually within 1%, however, in one case a difference of 2.6% was observed). Scales between runs did not differ more then 1.2% from unity. Extreme outliers (5.7% of the total data) were rejected during averaging, and reflections measured no more than twice were also discarded from the final data set. Other experimental details are listed in Table 1. A number of statistical measures of data quality obtained from the program *SORTAV*[16] are deposited. The values for R_{int} and the average $I/\sigma(I)$ in the various resolution shells suggest good data quality.

Table 1. Experimental Details

empirical formula	$C_{18}H_{22}O_2$
temperature (K)	20(2)
crystal size (mm^3)	0.20 × 0.20 × 0.10
crystal shape	prism
wavelength (Å)	0.710 73
crystal system	orthorhombic
space group	$P2_12_12_1$
unit cell dimensions (Å)	$a = 7.7358(1)$ $b = 9.9137(1)$ $c = 18.3572(2)$
V (Å^3), Z	1407.8, 4
μ (mm^{-1})	0.08
$(\sin\theta/\lambda)_{max}$ (Å^{-1})	1.331
reflections integrated	92 818
R_{int}[a]/average data multiplicity	0.0216/6.8
independent reflections	12 890
reflections used ($I > 4\sigma$, measured more than 2 times)	6883
refinement based on	F^2
total number of parameters	773
final $R(F^2)$ indices:	
spherical atom refinement	0.0673
aspherical atom refinement	0.0213
goodness of fit	1.05

[a] $R_{int} = \Sigma\sqrt{n/(n-1)}\Sigma|I - \bar{I}|/\Sigma\Sigma|I|$.

The estrone(II) crystal structure was first solved by Busetta et al.[9] The estrone molecule and crystal packing diagram showing a zigzag hydrogen bonding scheme similar to the one reported by Busetta et al. are shown in Figure 1. From our experimental data, the crystal structure was resolved by direct methods, and a preliminary least-squares refinement was carried out with the *SHELXTL* program suite.[17] The positions of hydrogen atoms at this stage were determined from the difference Fourier peaks. Anisotropic thermal motion was considered for all non-hydrogen atoms, and the latter were refined isotropically. A multipole model refinement [18] using the *XD* program package [19] was performed for both experimental and solid state theoretical (see below) data. The atomic standard local coordinate systems used to describe the electron density in estrogens have been previously reported.[20] To reduce correlations in the least-squares process, carbon atoms have been refined only up to the octapole level, while the oxygen atoms were refined up to hexadecapoles. To account for the hydrogen bonding in the crystal and the H−H intramolecular bonding (see below), all dipole and quadrupole parameters were refined for H(1A), H(1) (constrained to H(2, 4)), and H(11B) (constrained to H(11A)) atoms, while only the dipoles and one P_{20} quadrupole parameter were refined for all other hydrogens. Chemical constraints for similar carbon and hydrogen atoms were applied at the initial stages of refinements. Then, these constraints were gradually released, and the final model was refined unconstrained for the non-hydrogen atoms. The H(1, 2, 4), H(8, 9, 14), all H(A, B), and H(18(A, B, C)) were constrained to group values for the experimental data; however, no constraints were retained for the theoretical data. The molecular electroneutrality requirement has also been applied in each case. A total of nine expansion−contraction parameters, κ and κ', were utilized in order to allow the necessary

(9) Busetta, B.; Courseille, C.; Hospital, M. *Acta Crystallogr.* **1973**, *B29*, 298−313.
(10) Hardie, M. J.; Kirschbaum, K.; Martin, A.; Pinkerton, A. A. *J. Appl. Crystallogr.* **1998**, *31*, 815−817.
(11) Kirschbaum, K.; Martin, A.; Parrish, D.; Pinkerton, A. A. *J. Phys. Condens. Mater.* **1999**, *11*, 4483−4490.
(12) Ribaud, L.; Wu, G.; Zhang, Y.; Coppens, P. *J. Appl. Crystallogr.* **2001**, *34*, 76−79.
(13) Otwinowski, Z.; Minor, W. *Methods Enzymol.* **1997**, *276;* 307−326.
(14) Zhurov, V. V.; Zhurova, E. A.; Chen, Y.-S.; Pinkerton, A. A. *J. Appl. Crystallogr.* **2005**, *38*, 827−829.
(15) Zhurova, E. A.; Zhurov, V. V.; Tanaka, K. *Acta Crystallogr.* **1999**, *B55*, 917−922.
(16) Blessing, R. H. *Cryst. Rev.* **1987**, *1*, 3−58.
(17) Sheldrick, G. M. *SHELXTL, vers.6.14. An Integrated System for Solving, Refining and Displaying Crystal Structures from Diffraction Data*; University of Göttingen: Germany, 2000.
(18) Hansen, N.; Coppens, P. *Acta Crystallogr.* **1978**, *A34*, 909−921.
(19) Koritsanszky, T.; Richter, T.; Macchi, P.; Gatti, C.; Howard, S.; Mallinson, P. R.; Farrugia, L.; Su, Z. W.; Hansen, N. K. *XD − A Computer Program Package for Multipole Refinement and Analysis of Electron Densities from Diffraction Data*; Tech. Rep.; Freie Universität Berlin: Berlin, Germany, 2003.
(20) Kirschbaum, K.; Kumaradhas, P.; Parrish, D.; Pinkerton, A. A.; Zhurova, E. A. *J. Appl. Crystallogr.* **2003**, *36*, 1464−1466.

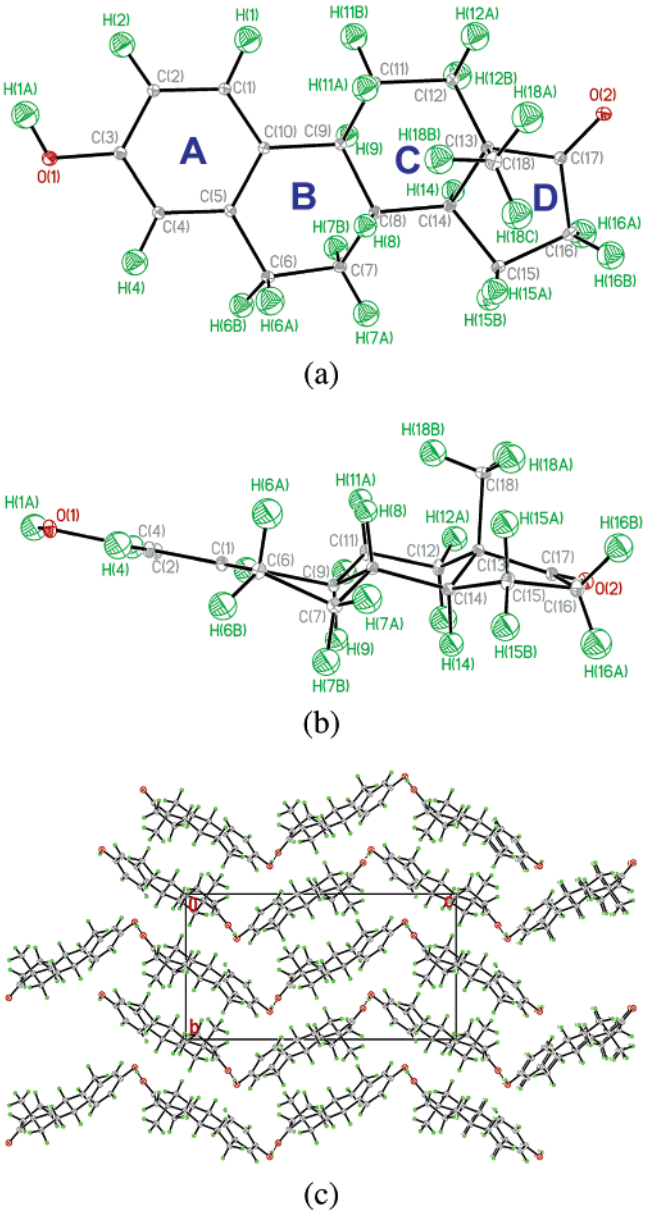

Figure 1. The top and side views of the estrone molecule showing 50% probability ellipsoids at 20 K (a, b) and estrone(II) crystal packing diagram viewed down the *a*-axis showing the ribbons formed by the hydrogen bonding scheme (c).

flexibility while attempting to maintain a minimum number of parameters (see Table 2). For the theoretical data, all κ and κ' values were freely refined including those for the hydrogen atoms. For the experimental data, the κ' set refined from the theoretical data was used, while κ values for all hydrogen atoms were fixed to 1.2. The O−H and C−H bond lengths were fixed to the tabulated values[21] according to their hybridization state. Highly correlated parameters were refined in separate groups; with the existing constraints (experimental data) the refinement procedure was stable, and full convergence of all parameters has been reached in each case.

From the experimental data, the rigid-bond test[22] showed that the differences of mean-square displacement amplitudes along the interatomic vectors were less than 7×10^{-4} Å^2. Averaged ratios of observed and calculated structure factors[23,14] were very close to unity indicating a correct scale factor for all data,[24] as well as good model fitting for

Table 2. Expansion/Contraction (κ and κ') Multipole Model Parameters

		κ		κ'	
atoms	no.	theory	expmt	theory	expmt
O(1)	1	0.995(1)	0.993(1)	1.122(1)	1.122
C(3)	2	0.991(2)	0.996(2)	0.842(9)	0.842
C(17)	3	0.989(2)	0.996(2)	0.866(8)	0.866
C(1), C(2), C(4)	4	1.002(1)	1.005(1)	0.916(8)	0.916
C(5), C(10)	5	1.000(2)	1.001(2)	0.875(8)	0.875
C(6),C(7),C(8),C(9),C(11), C(12),C(13),C(14), C(15),C(16),C(18)	6	1.003(1)	1.000(1)	0.881(3)	0.881
H(1A)	8	1.147(12)	1.200	1.416(40)	1.416
other H	7	1.173(3)	1.200	1.285(8)	1.285
O(2)	9	0.996(1)	0.991(1)	1.070(12)	1.070

the whole sin θ/λ range. The residual electron density (the difference between observed and calculated multipole electron densities: $\delta\rho_{\text{resid}} = \rho_{\text{exper}} - \rho_{\text{mult}}$) showed no peaks above or below 0.11/−0.09 eÅ^{-3} for the experimental data and 0.07/−0.07 eÅ^{-3} for the theoretical data (Figure 2). For the electron density analysis the program packages *XDPROP*,[19] *TOPXD*,[25] and *WinXPRO*[26,27] have been used.

The density functional theory (DFT) B3LYP periodic theoretical calculation was performed with the program *CRYSTAL98*.[28] The 6-31G-(d,p) basis set and a molecular geometry fixed at that observed experimentally[29] were used. The theoretical structure factors have been calculated for all possible *hkl* indices up to sin $\theta/\lambda = 1.0$ Å^{-1} and used for refinements in the same manner as that for the experimental data.

DFT molecular calculations were performed by obtaining the electron density of a single estrone molecule, frozen at the experimental geometry, at the B3LYP/6-311++G(d,p) level of theory. The resulting electron density was integrated using *PROAIM*,[30,31] and bond critical point data and the molecular graph were obtained by the use of *AIM 2000*.[32,33] *AIMDELOC*[34] was used to calculate the delocalization indices δ(A,B) between bonded atoms.[35] All AIM [36] atomic properties were obtained at the B3LYP/6-311++G(d,p)//(experimental geometry) level of theory except atomic energies to avoid the complications due to nonvanishing virials of the forces on the nuclei in a nonequilibrium geometry (vide infra).

To validate our discussion of atomic energies, we have also performed a careful full geometry optimization followed by a vibrational frequencies calculation all at the B3LYP/6-31G(d,p) level starting from the experimental geometry as an initial guess (the final maximum force and RMS force were as small as 0.000 006 and 0.000 001 hartrees/bohr, respectively). The absence of any negative frequencies was confirmed. A wave function at the same level of theory used in the

(21) Allen, F. H.; Kennard, O.; Watson, D. G.; Brammer, L.; Orpen, A. G.; Taylor, R. *J. Chem. Soc., Perkin Trans. 2*, **1987**, S1−S19.
(22) Hirshfeld, F. L. *Acta Crystallogr.* **1976**, *A32*, 239−244.
(23) Calculated with the program *XDRKplot* (courtesy of Dr. Stash, 2004).
(24) In the case of experimental data.
(25) Volkov, A.; Gatti, C.; Abramov, Yu.; Coppens, P. *Acta Crystallogr.* **2000**, *A56*, 252−258.
(26) Stash, A. I.; Tsirelson, V. G. *J. Appl. Crystallogr.* **2002**, *35*, 371−373.
(27) Stash, A. I.; Tsirelson, V. G. *Crystallogr. Rep.* **2005**, *50*, 202−209.
(28) Saunders, V. R.; Dovesi, R.; Roetti, C.; Causà, M.; Harrison, N. M.; Orlando, R.; Sicovich-Wilson, C. M. *CRYSTAL98 User's Manual*; University of Torino: Torino, 1998.
(29) After preliminary multipole refinements of the experimental data, the obtained molecular geometry was used for the theoretical solid state and molecular calculations.
(30) Bader, R. F. W. *AIMPAC.* http://www.chemistry.mcmaster.ca/aimpac/.
(31) Biegler-König F. W.; Bader R. F. W.; Tang T.-H. *J. Comput. Chem.* **1982**, *13*, 317−328.
(32) Biegler-König, F. W.; Schönbohm, J.; Bayles, D. http://gauss.fh-bielefeld.de/aim2000.
(33) Biegler-König, F. W.; Schönbohm, J.; Bayles, D. AIM2000 - A program to analyze and visualize atoms in molecules. *J. Comput. Chem.* **2001**, *22*, 545−559.
(34) Matta, C. F. *AIMDELOC: Program to calculate AIM localization and delocalization indices (QCPE0802)*; Quantum Chemistry Program Exchange, Indiana University: IN, 2001 (http://qcpe.chem.indiana.edu/).
(35) Fradera, X.; Austen, M. A.; Bader, R. F. W. *J. Phys. Chem.* **1999**, *A103*, 304−314.
(36) Atoms in molecules − refers to the Quantum Theory of Atoms in Molecules (AIM).

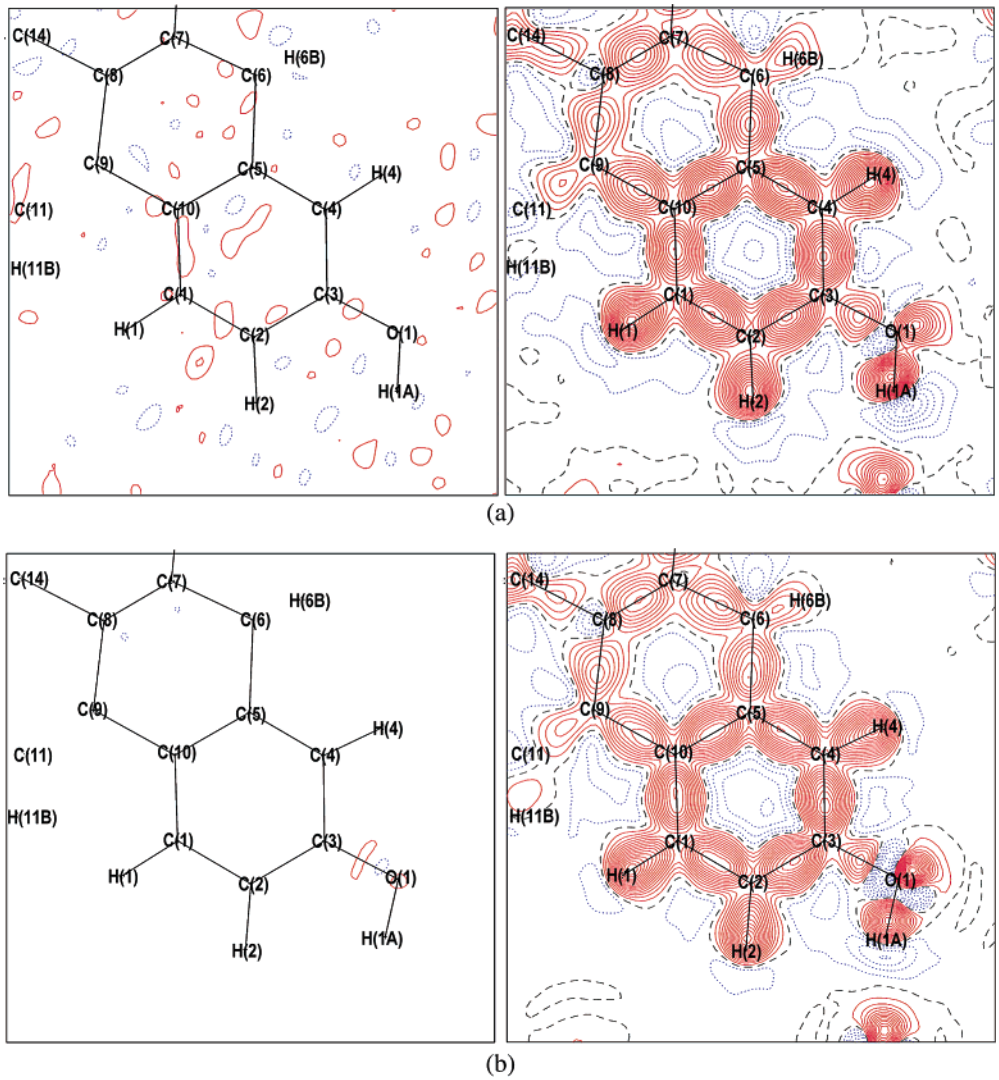

Figure 2. Residual electron density (left) and static multipole deformation density (right) in the A (aromatic) ring plane: (a) from the experimental data, (b) from the solid state theoretical data. Contour interval is 0.05 eÅ^{-3}; red solid lines are positive; blue dot lines are negative; black dash line is a zero contour. The Fourier series have been truncated at sin $\theta/\lambda = 1.0$ Å^{-1}. For clarity, the zero line is omitted from the residual maps.

geometry optimization was then obtained for the analysis of atomic energies [B3LYP/6-31G(d,p)//B3LYP/6-31G(d,p)].

Results and Discussion

An intramolecular interatomic distance which is important in preserving biological activity of estrogens is the O(1)···O(2) distance, which should range from ca. 10.3 Å to 12.1 Å for optimal estrogenic activity.[8] It has also been remarked that a distance of ca. 11 Å is very close to two β-helix turns in a polypeptide (2 × 5.38 Å) which corresponds to 7.5 amino acid residues [37] (at the rate of 3.6 residues per turn). In the present structure, we find these two oxygen atoms separated by 10.8325(4) Å, a value that does not change much upon geometry optimization at the B3LYP/6-31G(d,p) level at which it assumes the value of 10.8948 Å. The O···O distance we report here (whether experimental or optimized) is in very close agreement with those previously reported between the phenolic oxygen and O(17β) in two crystallographically independent estriol molecules where it assumes the values 10.952(7) Å and 11.085(7) Å,[37] in 4-bromo-estrone where it is 10.78(4) Å,[37] and in the estradiol molecule where it is in the range 10.863−11.226 Å.[38,39]

Multipole and Topological Analysis of the Electron Density. Static multipole electron density maps are shown in Figures 2 and 3. There is a very good qualitative agreement between the experimental and theoretical (solid state calculation with the multipole model refined) results, except for the lone pair region of the O(2) atom, which appeared to be more polarized in the experimental case. All the expected features of covalent bonding and oxygen lone pair regions are clearly seen, as well as the polarization of the electron density indicating the hydrogen H(1A)···O(2) bond[40] (Figure 3).

The hydroxyl H(1A) atom lays almost in the aromatic ring plane with a deviation of 0.03 Å from the A-ring mean plane (Figure 1). It could be expected in this case that the hydroxyl group would be of sp^2 type geometry having some interaction with the π-orbitals of the aromatic ring. Although the electron density of the lone pair regions of both oxygen atoms is

(37) Cooper, A.; Norton, D. A.; Hauptman, H. *Acta Crystallogr.* **1969**, *B25*, 814−828.
(38) Kirschbaum, K.; Parrish, D.; Pinkerton, A. A.; Zhurova, E. A. To be published, 2006.
(39) Cambridge Structural Data Base, 2005.
(40) Krijn, M. P. C. M.; Graafsma, H.; Feil, D. *Acta Crystallogr.* **1988**, *B44*, 609−616.

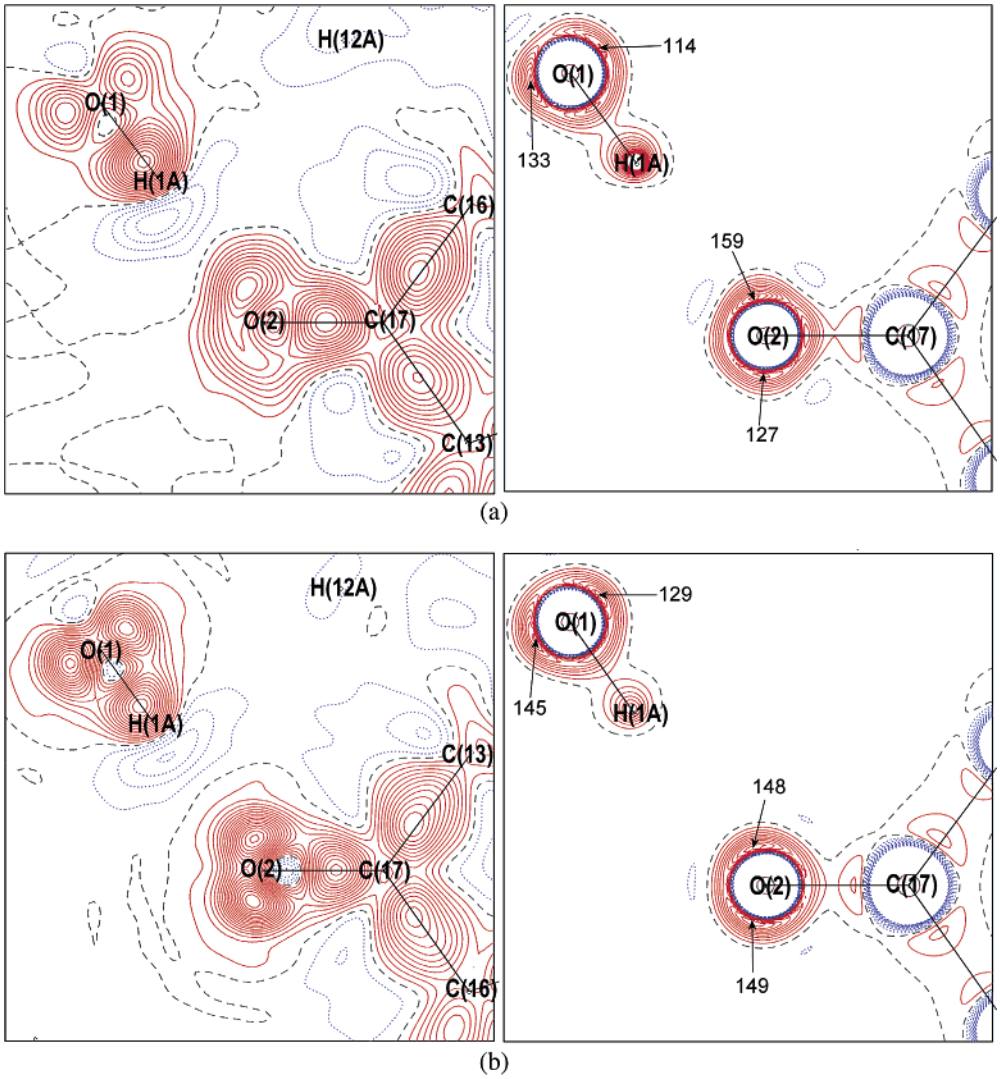

Figure 3. Static multipole deformation density (left) and the Laplacian of the total electron density (right) in the O(2)−C(17)···O(1) ($0.5 - x - 3$, $-y - 1$, $0.5 + x - 1$) plane: (a) from the experimental data, (b) from the solid state theoretical data. The deformation density isocontours and the Fourier series truncation are as those in Figure 2. The Laplacian contour interval is 15 eÅ^{-5}, negative $\nabla^2\rho(\mathbf{r})$ contours are red, and positive contours are blue. Numbers on the maps correspond to the values at the maxima in the negative Laplacian.

somewhat smeared, both the deformation electron density and the Laplacian ($\nabla^2\rho(\mathbf{r})$) maps (Figure 3) demonstrate two nonbonding concentrations of electron density for each atom, i.e., two lone pairs. The existence of two charge concentrations in the lone pair region is, probably, an indication that the interaction of the hydroxyl oxygen orbitals with the π-orbitals of the aromatic ring is not very significant.

Bond critical points in the electron density [41] associated with shared (covalent) intramolecular bonding are listed in Table 3. A very good agreement between experiment and theory is also observed. Every chemical bond is represented with a (3,−1) bond critical point with a high electron density value and a negative Laplacian. The double O(2)−C(17) bond has the highest electron density but is not significantly elliptical. The bonds in the aromatic ring have much higher electron density at the bond critical point ($\rho_b = 2.12$ eÅ^{-3} when averaged over the six bonds in ring **A** in estrone[42]) and much higher ellipticities ($\epsilon = 0.21$ again, when averaged over the six bonds in ring **A** in estrone[42]) than those of the rest of the C−C bonds in estrone. These values are not much different than the values of $\rho_b = 2.08$ eÅ^{-3} and $\epsilon = 0.20$ we calculated for the benzene molecule at the B3LYP/6-311++G(d,p)//B3LYP/6-311++G(d,p) level of theory. (For comparison, the average value of the electron density in single C−C bonds in estrone is 1.67 eÅ^{-3}, and the average ellipticity, 0.05.) The polarization of the C−O, O−H, and C−H bonds is evident, the C−C bonds being less polarized. All these values are in the expected range found in the literature (see, for example, refs 43−49).

The molecular calculation results are generally in excellent agreement with both the experimental and the periodic calculation results, as can be seen from Table 3. The largest discrepancies between the three sets of results in Table 3 are in the values of the Laplacian, $\nabla^2\rho_b$.

(41) Bader, R. F. W. *Atoms in Molecules: A Quantum Theory*; Oxford: Clarendon Press, 1990.
(42) From the experimental data.
(43) Destro, R.; Merati, F. *Z. Naturforsch.* **1993**, *48a*, 99−104.
(44) Li, X.; Wu, G.; Abramov, Yu. A.; Volkov, A. V.; Coppens, P. *Proc. Natl. Acad. Sci. U.S.A.* **2002**, *99*, 12132−12137.
(45) Ellena, J.; Goeta, A. E.; Howard, J. A. K.; Punte, G. *J. Phys. Chem.* **2001**, *A105*, 8696−8708.
(46) Hibbs, D. E.; Hanrahan, J. R.; Hursthouse, M. B.; Knight, D. W.; Overgaard, J.; Turner, P.; Piltz, R. O.; Waller, M. P. *Org. Biomol. Chem.* **2003**, *1*, 1034−1040.

Table 3. Bond Critical Points in the Electron Density: Covalent Bonds[a]

bond path	ρ, eÅ^{-3}	$\nabla^2\rho$, eÅ^{-5}	λ, eÅ^{-5}	λ_2, eÅ^{-5}	λ_3, eÅ^{-5}	ϵ	d_1, Å	d_2, Å	R, Å	δ(A,B)
O(1)−C(3)	2.036	−15.93	−15.041	−14.087	13.202	0.068	0.829	0.537	1.365	-
	2.003	−16.35	−14.900	−13.738	12.284	0.085	0.826	0.539	-	-
	1.924	−9.21	−13.863	−13.765	18.415	0.007	0.900	0.466	-	0.935
O(2)−C(17)	2.856	−17.56	−26.594	−25.268	34.300	0.052	0.805	0.416	1.221	-
	2.814	−24.50	−25.454	−24.187	25.136	0.052	0.796	0.425	-	-
	2.706	−4.06	−24.525	−23.836	44.307	0.029	0.804	0.417	-	1.445
C(1)−C(2)	2.146	−17.68	−15.792	−13.204	11.313	0.196	0.704	0.690	1.393	-
	2.091	−17.33	−15.291	−12.855	10.820	0.189	0.692	0.701	-	-
	2.077	−20.45	−15.548	−12.741	7.844	0.220	0.695	0.698	-	1.396
C(1)−C(10)	2.053	−16.98	−15.166	−12.426	10.616	0.220	0.679	0.723	1.403	-
	2.075	−17.22	−15.341	−12.482	10.607	0.229	0.698	0.705	-	-
	2.044	−19.72	−15.179	−12.529	7.987	0.211	0.707	0.696	-	1.350
C(2)−C(3)	2.152	−19.34	−16.018	−13.447	10.122	0.191	0.691	0.706	1.397	-
	2.127	−19.17	−15.988	−12.869	9.688	0.242	0.674	0.724	-	-
	2.081	−20.61	−15.780	−12.697	7.865	0.243	0.676	0.722	-	1.311
C(3)−C(4)	2.130	−19.08	−15.962	−12.894	9.774	0.238	0.734	0.661	1.395	-
	2.136	−19.30	−16.143	−12.680	9.525	0.273	0.734	0.661	-	-
	2.100	−21.09	−16.068	−12.872	7.849	0.248	0.730	0.665	-	1.316
C(4)−C(5)	2.146	−18.66	−16.131	−13.185	10.657	0.223	0.688	0.714	1.402	-
	2.072	−16.88	−15.188	−12.371	10.684	0.228	0.693	0.709	-	-
	2.042	−19.65	−15.134	−12.429	7.913	0.218	0.703	0.699	-	1.361
C(5)−C(10)	2.101	−18.69	−15.824	−13.083	10.217	0.210	0.705	0.705	1.410	-
	2.047	−16.79	−15.049	−12.177	10.438	0.236	0.708	0.702	-	-
	2.019	−19.09	−14.925	−12.235	8.071	0.220	0.712	0.698	-	1.330
C(5)−C(6)	1.681	−11.06	−11.454	−10.395	10.786	0.102	0.774	0.742	1.516	-
	1.637	−9.53	−10.643	−9.956	11.067	0.069	0.778	0.738	-	-
	1.681	−14.04	−11.553	−11.087	8.597	0.042	0.773	0.743	-	0.991
C(6)−C(7)	1.672	−10.04	−10.746	−10.382	11.091	0.035	0.762	0.766	1.528	-
	1.621	−9.35	−10.348	−10.089	11.091	0.026	0.770	0.758	-	-
	1.636	−13.22	−10.925	−10.896	8.600	0.003	0.769	0.759	-	0.978
C(7)−C(8)	1.684	−10.35	−10.922	−10.483	11.051	0.042	0.760	0.766	1.526	-
	1.627	−9.49	−10.362	−10.145	11.016	0.021	0.750	0.776	-	-
	1.652	−13.33	−11.047	−11.000	8.717	0.004	0.762	0.764	-	0.960
C(8)−C(9)	1.598	−8.68	−9.940	−9.773	11.030	0.017	0.783	0.762	1.545	-
	1.587	−8.61	−10.044	−9.684	11.114	0.037	0.771	0.774	-	-
	1.606	−12.55	−10.668	−10.576	8.695	0.009	0.771	0.773	-	0.938
C(8)−C(14)	1.691	−11.05	−11.014	−10.737	10.705	0.026	0.730	0.792	1.522	-
	1.657	−9.99	−10.612	−10.392	11.014	0.021	0.747	0.776	-	-
	1.668	−13.60	−11.201	−11.141	8.747	0.005	0.756	0.766	-	0.956
C(9)−C(10)	1.700	−10.62	−11.295	−10.500	11.177	0.076	0.740	0.786	1.526	-
	1.616	−9.42	−10.695	−9.734	11.013	0.099	0.744	0.782	-	-
	1.648	−13.38	−11.210	−10.747	8.573	0.043	0.752	0.774	-	0.976
C(9)−C(11)	1.652	−9.94	−10.643	−10.361	11.061	0.027	0.765	0.776	1.541	-
	1.597	−8.77	−10.168	−9.776	11.175	0.040	0.770	0.771	-	-
	1.605	−12.51	−10.673	−10.519	8.687	0.015	0.775	0.765	-	0.954
C(11)−C(12)	1.607	−9.11	−10.301	−9.829	11.023	0.048	0.763	0.779	1.542	-
	1.554	−8.14	−9.684	−9.543	11.087	0.015	0.778	0.764	-	-
	1.592	−12.37	−10.508	−10.439	8.573	0.007	0.774	0.768	-	0.967
C(12)−C(13)	1.657	−10.21	−10.800	−10.281	10.870	0.050	0.768	0.758	1.526	-
	1.622	−9.42	−10.402	−10.030	11.014	0.037	0.759	0.767	-	-
	1.648	−13.31	−11.040	−10.934	8.662	0.010	0.754	0.773	-	0.956
C(13)−C(14)	1.606	−9.05	−10.085	−9.856	10.889	0.023	0.779	0.765	1.544	-
	1.580	−8.57	−9.801	−9.753	10.986	0.005	0.776	0.767	-	-
	1.616	−12.56	−10.722	−10.591	8.750	0.012	0.774	0.770	-	0.922
C(13)−C(17)	1.759	−12.00	−11.852	−10.862	10.712	0.091	0.717	0.799	1.515	-
	1.749	−12.05	−11.657	−10.935	10.543	0.066	0.715	0.800	-	-
	1.744	−14.89	−12.309	−11.814	9.233	0.042	0.737	0.779	-	0.912
C(13)−C(18)	1.553	−8.46	−9.724	−9.539	10.807	0.019	0.768	0.779	1.546	
	1.541	−8.01	−9.593	−9.381	10.965	0.023	0.782	0.764	-	-
	1.552	−11.60	−10.087	−9.900	8.383	0.019	0.778	0.769	-	-
C(14)−C(15)	1.620	−9.23	−10.486	−9.810	11.064	0.069	0.761	0.778	1.539	-
	1.588	−8.65	−10.025	−9.735	11.114	0.030	0.763	0.776	-	-
	1.608	−12.47	−10.611	−10.546	8.689	0.006	0.766	0.774	-	0.952

Table 3. (Continued)[a]

bond path	ρ, eÅ^{-3}	$\nabla^2\rho$, eÅ^{-5}	λ, eÅ^{-5}	λ_2, eÅ^{-5}	λ_3, eÅ^{-5}	ϵ	d_1, Å	d_2, Å	R, Å	δ(A,B)
C(15)−C(16)	1.560	−8.16	−9.789	−9.527	11.158	0.028	0.759	0.788	1.547	-
	1.532	−7.80	−9.501	−9.412	11.113	0.009	0.759	0.788	-	-
	1.577	−12.12	−10.343	−10.282	8.501	0.006	0.766	0.781	-	0.968
C(16)−C(17)	1.687	−10.54	−11.229	−10.359	11.047	0.084	0.740	0.787	1.527	-
	1.674	−10.59	−11.104	−10.275	10.792	0.081	0.729	0.798	-	-
	1.684	−13.88	−11.73	−11.193	9.082	0.052	0.748	0.779	-	0.926
O(1)−H(1A)	2.656	−48.36	−43.167	−41.491	36.295	0.040	0.723	0.249	0.967	-
	2.523	−51.95	−42.240	−41.445	31.740	0.019	0.738	0.229	-	-
	2.458	−59.93	−42.597	−41.634	24.296	0.023	0.768	0.177	-	0.677
C(1)−H(1)	1.916	−18.64	−17.695	−16.253	15.304	0.089	0.666	0.418	1.083	-
	1.912	−19.83	−17.665	−17.382	15.213	0.016	0.689	0.394	-	-
	1.907	−23.38	−18.116	−17.775	12.506	0.019	0.691	0.377	-	0.944
C(2)−H(2)	1.843	−16.76	−16.372	−15.276	14.886	0.072	0.657	0.426	1.083	-
	1.865	−18.58	−17.216	−16.358	14.996	0.052	0.684	0.399	-	-
	1.880	−22.73	−17.654	−17.171	12.091	0.028	0.688	0.381	-	0.962
C(4)−H(4)	1.867	−17.72	−16.841	−15.659	14.779	0.075	0.659	0.424	1.083	
	1.890	−19.63	−17.583	−16.869	14.820	0.042	0.685	0.398	-	
	1.892	−23.04	−18.009	−17.539	12.513	0.027	0.693	0.375	-	0.948
C(6)−H(6A)	1.841	−17.12	−15.489	−15.069	13.440	0.028	0.649	0.446	1.092	-
	1.836	−17.68	−16.238	−15.935	14.497	0.019	0.683	0.409	-	-
	1.858	−22.00	−17.090	−16.953	12.042	0.008	0.692	0.386	-	0.930
C(6)−H(6B)	1.847	−16.77	−15.438	−15.141	13.809	0.020	0.652	0.442	1.092	-
	1.864	−18.60	−16.506	−16.378	14.287	0.008	0.683	0.409	-	-
	1.862	−22.15	−17.225	−17.060	12.134	0.010	0.693	0.385	-	0.937
C(7)−H(7A)	1.819	−14.68	−15.379	−15.098	15.798	0.019	0.676	0.418	1.092	-
	1.806	−15.50	−15.773	−15.475	15.749	0.019	0.693	0.399	-	-
	1.863	−22.17	−17.121	−17.068	12.018	0.003	0.691	0.387	-	0.938
C(7)−H(7B)	1.770	−14.36	−14.808	−14.665	15.113	0.010	0.668	0.427	1.092	-
	1.837	−16.93	−16.643	−15.866	15.577	0.049	0.699	0.393	-	-
	1.862	−22.13	−17.101	−17.037	12.012	0.004	0.691	0.387	-	0.934
C(8)−H(8)	1.783	−15.17	−15.301	−15.040	15.167	0.017	0.684	0.418	1.099	-
	1.826	−17.77	−16.168	−15.878	14.277	0.018	0.686	0.413	-	-
	1.844	−21.57	−16.742	−16.720	11.893	0.001	0.694	0.392	-	0.901
C(9)−H(9)	1.772	−14.86	−15.005	−14.910	15.050	0.006	0.682	0.419	1.099	-
	1.831	−17.83	−16.188	−15.886	14.243	0.019	0.687	0.412	-	-
	1.841	−21.50	−16.769	−16.684	11.953	0.005	0.695	0.391	-	0.904
C(11)−H(11A)	1.808	−15.92	−15.632	−15.196	14.913	0.029	0.676	0.420	1.092	-
	1.793	−15.10	−15.588	−15.259	15.752	0.022	0.693	0.399	-	-
	1.866	−22.12	−17.151	−17.031	12.058	0.007	0.691	0.388	-	0.929
C(11)−H(11B)	1.819	−16.66	−15.969	−15.388	14.697	0.038	0.676	0.421	1.092	-
	1.857	−18.32	−16.618	−16.213	14.513	0.025	0.684	0.408	-	-
	1.865	−22.16	−17.119	−17.040	12.001	0.005	0.690	0.388	-	0.927
C(12)−H(12A)	1.844	−15.43	−15.653	−14.857	15.076	0.054	0.660	0.435	1.092	-
	1.867	−18.92	−16.775	−16.490	14.345	0.017	0.685	0.407	-	-
	1.868	−22.30	−17.338	−17.267	12.302	0.004	0.695	0.383	-	0.936
C(12)−H(12B)	1.815	−14.91	−15.307	−14.276	14.670	0.072	0.655	0.440	1.092	-
	1.848	−17.99	−16.310	−16.104	14.422	0.013	0.681	0.411	-	-
	1.865	−22.22	−17.222	−17.125	12.127	0.006	0.693	0.385	-	0.933
C(14)−H(14)	1.810	−15.90	−15.601	−15.452	15.148	0.010	0.685	0.416	1.099	-
	1.846	−18.14	−16.344	−16.022	14.255	0.020	0.684	0.415	-	-
	1.845	−21.56	−16.737	−16.676	11.854	0.004	0.694	0.392	-	0.906
C(15)−H(15A)	1.769	−14.11	−15.187	−14.806	15.884	0.026	0.691	0.405	1.092	-
	1.801	−15.37	−15.581	−15.500	15.711	0.005	0.693	0.399	-	-
	1.863	−22.07	−17.108	−17.042	12.082	0.004	0.691	0.387	-	0.937
C(15)−H(15B)	1.789	−14.79	−15.702	−15.019	15.927	0.045	0.692	0.403	1.092	-
	1.793	−15.64	−15.618	−15.550	15.533	0.004	0.695	0.397	-	-
	1.863	−22.16	−17.191	−17.133	12.168	0.003	0.693	0.385	-	0.947
C(16)−H(16A)	1.774	−13.71	−15.232	−14.270	15.795	0.067	0.680	0.415	1.092	-
	1.773	−15.01	−15.574	−15.067	15.628	0.034	0.698	0.394	-	-
	1.843	−21.68	−17.082	−16.763	12.169	0.019	0.696	0.382	-	0.937
C(16)−H(16B)	1.779	−13.68	−15.195	−14.506	16.020	0.048	0.683	0.413	1.092	-
	1.778	−15.66	−15.784	−15.148	15.277	0.042	0.696	0.396	-	-
	1.845	−21.73	−17.154	−16.815	12.240	0.020	0.697	0.381	-	0.935

Table 3. (Continued)[a]

bond path	ρ, eÅ^{-3}	$\nabla^2\rho$, eÅ^{-5}	λ, eÅ^{-5}	λ_2, eÅ^{-5}	λ_3, eÅ^{-5}	ϵ	d_1, Å	d_2, Å	R, Å	δ(A,B)
C(18)−H(18A)	1.817	−14.80	−15.761	−14.446	15.404	0.091	0.651	0.409	1.059	-
	1.913	−18.36	−17.178	−16.515	15.332	0.040	0.669	0.390	-	-
	1.986	−24.95	−18.729	−18.613	12.392	0.006	0.667	0.377	-	0.934
C(18)−H(18B)	1.792	−14.74	−15.655	−13.971	14.884	0.120	0.647	0.415	1.059	-
	1.913	−18.09	−16.830	−16.611	15.348	0.013	0.666	0.393	-	-
	1.986	−25.08	−18.885	−18.679	12.486	0.011	0.670	0.375	-	0.953
C(18)−H(18C)	1.791	−13.77	−15.351	−13.835	15.421	0.110	0.650	0.411	1.059	-
	1.942	−19.40	−17.568	−16.926	15.098	0.038	0.667	0.392	-	-
	1.980	−24.90	−18.695	−18.448	12.244	0.013	0.667	0.378	-	0.950

[a] First line, experimental; second line, solid state theoretical calculation and multipole model refined; third line, molecular theoretical calculation at the B3LYP/6-311++G(d,p)//(experimental geometry) level of theory. ρ is the electron density; $\nabla^2\rho$ is the Laplacian; λ_1, λ_2, λ_3 are the principle curvatures; $\epsilon = (\lambda_1/\lambda_2) - 1$ is the bond ellipticity; d_1, d_2 are the distances from the critical point to atoms 1 and 2; R is the interatomic distance (entered only in the row of the experimental values since the geometry in each theoretical calculation was frozen at the experimental geometry); δ(A,B) is the electron delocalization index (calculated only in the case of the molecular calculation).

The number of electron pairs shared between two bonded atoms is known to chemists as the bond order. Fradera, Austen, and Bader define a delocalization index which counts the number of pairs shared between any two atoms in a molecule (bonded or not) by integrating the exchange density once over each of the two atomic basins.[35] When the delocalization index is reported for two *bonded* atoms it is, therefore, a measure of the bond order between them.[35]

The delocalization index $\delta(A,B)$ between atoms A and B is defined, in terms of the magnitude of the exchange of the electrons in the basin of atom A with those in the basin of atom B, as

$$\delta(A,B) = 2|F^{\alpha}(A,B)| + 2|F^{\beta}(A,B)| \quad (1)$$

where

$$F^{\sigma}(A,B) = -\sum_i \sum_j \int_A d\mathbf{r}_1 \int_B d\mathbf{r}_2 \{\phi_i^*(\mathbf{r}_1)\phi_j(\mathbf{r}_1)\phi_j^*(\mathbf{r}_2)\phi_i(\mathbf{r}_2)\}$$
$$= -\sum_i \sum_j S_{ij}(A)\, S_{ji}(B) \quad (2)$$

where $S_{ij}(X) = S_{ji}(X)$ is the overlap integral of two spin−orbitals over a region A, and σ represents α- or β-spin.

As suggested previously,[50] one can calibrate Bader's bond order equation ($n = \exp[A(\rho_b - B)]$) to reproduce the delocalization indices[35] between bonded carbon atoms, δ(C,C′), which provide a physical measure of the bond order when calculated between atoms sharing a bond path. In this way, one can empirically obtain information such as δ(C,C′) which is only contained in a density *matrix* (as opposed to just its diagonal elements, the electron density), from an experimental electron density. Strictly speaking, DFT provides only the ground-state electron density, not a density matrix, but because of the formal similarity of the Kohn−Sham (KS) implementation of density functional theory to the Hartree−Fock theory, one can use a DFT Slater determinant to calculate the delocalization indices (see discussion in ref 51 and references therein). The KS delocalization indices are usually slightly higher (rather than lower, as they should be) than the Hartree−Fock indices. (See discussions in refs 52 and 53 and references therein.) Using the experimental ρ_{BCP} (in au) for the 21 C−C bonds in the estrone, we obtain

$$\delta(C,C') = \exp[A(\rho_{BCP} - B)] \quad (3)$$

where $A = 4.7427$, $B = 0.2538$, $r^2 = 0.939$, variance = 0.002, RMSD = 0.010, and an average absolute deviation of 0.032 between the fitted and directly calculated δ(C,C′). This provides the first example of a correlation between the calculated AIM delocalization indices, a quantity which requires a density matrix, and the one-electron density obtained from experiment.

The aromatic character of estrone, and estrogens in general, is essential for estrogenic activity.[8] In fact, an essential step in an estrogen's biosynthesis is the loss of a methyl group (C(19)) from the C(10) position of an androgen, namely, androstenedione or testosterone, followed by the aromatization of ring **A** to yield estrone or estradiol, respectively.[8] This aromatization and loss of a carbon unit is catalyzed by cytochrome P450 aromatase enzyme.[54] Furthermore, the aromaticity of ring **A** (*and only* ring **A**) in estrogens and estrogen analogues has been shown to be essential for the retention of a significant inhibitory allosteric effect on glutamate dehydrogenase.[55] The **A** ring's aromatic character is decreased due to geometrical distortions or alternation of bond lengths and bond orders. Consistent with the observations of Busetta et al.,[9] the aromatic ring angle C(5)−C(10)−C(1) is too closed with respect to the ideal 120°, its value being 117.87(3)°, while the five remaining aromatic ring angles vary between 122.18(3)° and 119.40(3)°. Bond lengths also fluctuate around the aromatic ring **A**, their values falling between 1.4102(5) Å [C(5)−C(10] and 1.3932(5) Å [C(1)−C(2)]. These geometrical distortions are reflected in the fluctuation of the C−C bond order around the aromatic ring with the highest δ-[C(1),C(2)] = 1.396 and the lowest δ[C(2),C(3)] = 1.311, to be compared to benzene where δ(C,C′) = 1.389 at the B3LYP/6-311++G(d,p)//B3LYP/6-311++G(d,p) level of theory.

(47) Dominiak, P. M.; Grech, E.; Barr, G.; Teat, S.; Mallinson, P.; Wozniak, K. *Chem.—Eur. J.* **2003**, *9*, 963−970.
(48) Scheins, S.; Messerschmidt, M.; Luger, P. *Acta Crystallogr.* **2005**, *B61*, 443−448.
(49) Messerschmidt, M.; Scheins, S.; Luger, P. *Acta Crystallogr.* **2005**, *B61*, 115−121.
(50) Matta, C. F.; Hernández-Trujillo, J. *J. Phys. Chem.* **2003**, *A107*, 7496−7504 (Correction: *J. Phys. Chem.* **2005**, *A107*, 10798).
(51) Poater, J.; Solà, M.; Duran, M.; Fradera, X. *Theor. Chem. Acc.* **2002**, *107*, 362−371.
(52) Fradera, X.; Poater, J.; Simon, S.; Duran, M.; Solà, M. *Theor. Chem. Acc.* **2002**, *108*, 214−224.
(53) Wang, Y.-G.; Werstiuk, N. H. *J. Comput. Chem.* **2003**, *24*, 379−385.
(54) Simpson, E. R.; Mahendroo, M. S.; Means, G. D.; Kilgore, M. W.; Hinshelwood, M. M.; Graham-Lorence, S.; Amarneh, B.; Ito, Y.; Fisher, C. R.; Michael, M. D.; Mendelson, C. R.; Bulun, S. E. *Endocr. Rev.* **1994**, *15*, 342−355.
(55) Pons, M.; Michel, F.; Descomps, B.; Crastes de Paulet, A. *Eur. J. Biochem.* **1978**, *84*, 257−266.

Table 4. Bond Critical Points in the Electron Density: H−H and Hydrogen Bonds[a]

bond path	ρ, eÅ^{-3}	$\nabla^2\rho$, eÅ^{-5}	λ_1, eÅ^{-5}	λ_2, eÅ^{-5}	λ_3, eÅ^{-5}	d_1, Å	d_2, Å	R, Å	g, au	v, au	h_e, au	δ(A,B)
H(1)−H(11B)	0.077	1.23	−0.250	−0.179	1.656	1.098	1.117	2.090	0.010	−0.008	0.003	-
	0.081	1.18	−0.319	−0.147	1.651	1.064	1.053	2.090	0.010	−0.008	0.002	-
	0.085	1.12	−0.297	−0.172	1.587	1.099	1.109	2.090	0.009	−0.007	0.002	0.027
H(8)−H(18A)	-	-	-	-	-	-	-	-	-	-	-	-
	-	-	-	-	-	-	-	-	-	-	-	-
	0.078	1.04	−0.245	−0.105	1.388	1.133	1.181	2.104	0.009	−0.007	0.002	0.022
H(11A)−H(18A)	-	-	-	-	-	-	-	-	-	-	-	-
	-	-	-	-	-	-	-	-	-	-	-	-
	0.073	1.01	−0.231	−0.044	1.283	1.298	1.148	2.136	0.009	−0.007	0.002	0.021
O(2)···H(1A)	0.208	2.01	−1.369	−1.269	4.643	1.198	0.659	1.842	0.023	−0.024	−0.002	-
	0.217	1.57	−1.351	−1.269	4.193	1.197	0.656	1.842	0.020	−0.024	−0.004	-
	-	-	-	-	-	-	-	-	-	-	-	-

[a] First line, experimental; second line, solid state theoretical calculation and multipole model refined; third line, molecular theoretical calculation at the B3LYP/6-311++G(d,p)//(experimental geometry) level of theory. ρ is the electron density; $\nabla^2\rho$ is the Laplacian; λ_1, λ_2, λ_3 are the principle curvatures; d_1, d_2 are the distances from the critical point to atoms 1 and 2; R is the interatomic distance; g, v and h_e are the kinetic, potential, and total electronic energy densities; δ(A,B) is electron delocalization index (calculated only in the case of the molecular calculation).

The bond order and bond length alternation in a ring are indicators of loss of aromatic character. We have used the delocalization indices to quantify the degree of aromaticity of the phenolic ring of estrone according to the aromaticity criterion θ, defined[50] as

$$\theta = 1 - \frac{c}{n}\sqrt{\sum_{i=1}^{n}(\delta_0 - \delta_i)^2} \qquad (4)$$

where $n = 6$ and, at the B3LYP/6-311++G(d,p) level of theory, $c = 2.4993$ is a constant such that $\theta = 0$ for cyclohexane ($\theta = 1$ for benzene, by definition), $\delta_0 = 3.0264$ is the total electron delocalization of a carbon atom of benzene with all other C atoms in that molecule, and δ_i is the total electron delocalization of a carbon atom in the ring with the other carbon atoms of the ring. With these values we find $\theta = 0.880$, an aromaticity closer to that of the outer rings in phenanthrene ($\theta = 0.863$) and dibenz[*a*,*j*]anthracene ($\theta = 0.877$) rather than the closely associated molecule 9,10-dihydrophenanthrene ($\theta = 0.942$). This last observation can be due to a substituent effect, whereby conjugation with the phenolic group participates in a slight reduction of the aromaticity of the ring.

A relatively short (1.84 Å) O(2)···H(1A) hydrogen bond is found in the estrone structure featuring the zigzag crystal packing (Figure 1c). Corresponding bond critical point parameters are listed in Table 4, where g, v, and h_e are the kinetic, potential, and total electronic energy densities calculated from the electron density and its derivatives using the DFT functionals and the local virial theorem.[56−61] The O(2)···H(1A) interaction is characterized by a relatively high electron density value and a positive Laplacian. A negative electronic energy density and accordingly $|v|/g > 1$, as well as a bond degree parameter,[62,63] h_e/ρ (−0.0087 and −0.0180 for the experimental and theoretical data, respectively), suggest incipient (incomplete) covalent bonding or partially covalent character of this hydrogen bond.[64]

Hydrogen−Hydrogen Interaction. One of the most interesting features of the estrone molecule is the formation of an intramolecular H(1)−H(11B) chemical bond. The hydrogen−hydrogen bonding interaction has been found in several compounds before; see, for example, refs 65 and 66 and references therein. This interaction is characterized by relatively high electron density at the critical point, positive Laplacian, and positive electronic energy density, which are indicators of the closed-shell character of this interaction (Table 4). The H(1)···H(11B) distance is found to be 2.089(11) Å, a distance that is slightly changed in the optimized geometry (2.056 Å), values significantly shorter than the double of the van der Waals radius of the hydrogen atom[67] (2.4 Å). A (3,−1) critical point in the electron density (Table 4), a bond path (Figure 4), and a virial path in the (negative) potential energy density field[68] strongly suggest the bonding character of this interaction in the estrone molecule. A significant *local* stabilization has been ascribed to this type of bonding wherein each hydrogen atom can be stabilized by up to ca. 2−7 kcal/mol.[65,66] As will be seen below, H(1) and H(11B) are indeed more stable than comparable hydrogen atoms in estrone.

Table 5 lists atomic charges and volumes integrated over the atomic basins delimited by the zero-flux surfaces[41] for the experimental and both theoretical cases and the atomic energies relative to the free atomic ground states of each element. The atomic properties of H(1) and H(11B) are typical of hydrogen atoms involved in a H−H bonding interaction. Most importantly, because both H(1) and H(11B) are practically electrically neutral (or carry insignificant charges), one cannot identify their interaction as a dihydrogen bond since it lacks a proton donor and an acceptor, or, equivalently, a pair of hydrogen atoms bearing opposite charges of significant magnitudes. Furthermore,

(56) Kirzhnits, D. A. *Sov. Phys. JETP* **1957**, *5*, 64−71.
(57) Abramov, Y. A. *Acta Crystallogr.* **1997**, *A53*, 264−272.
(58) Tsirelson, V. G. *Acta Crystallogr.* **2002**, *B58*, 632−639.
(59) Espinosa, E.; Molins, E.; Lecomte, C. *Chem. Phys. Lett.* **1998**, *285*, 170−173.
(60) Espinosa, E.; Lecomte, C.; Molins, E. *Chem. Phys. Lett.* **1999**, *300*, 745−748.
(61) Espinosa, E.; Molins, E. *J. Chem. Phys.* **2000**, *11*, 5686−5694.
(62) A bond degree parameter (BD), h_e/ρ, expresses the total energy per electron an the bond critical point. The greater BD is, the more covalent and stronger the bond is.
(63) Espinosa, E.; Alkorta, I.; Elguero, J.; Molins, E. *J. Chem. Phys.* **2002**, *117*, 5529−5542.
(64) Gatti, C. *Z. Kristallogr.* **2005**, *220*, 399−457.
(65) Matta, C. F.; Hernandez-Trujillo, J.; Tang, T.-H.; Bader, R. F. W. *Chem.−Eur. J.* **2003**, *9*, 1940−1951.
(66) Matta, C. F. In *Hydrogen Bonding − New Insight*; Grabowski, S., Ed.; Challenges and Advances in Computational Chemistry and Physics Series; Springer: 2006; pp 337−376.
(67) Pauling, L. *The Nature of the Chemical Bond*, 3rd ed.; Cornell University Press: Ithaca, NY, 1960.
(68) Bader, R. W. F. *J. Phys. Chem.* **1998**, *A102*, 7314−7323.

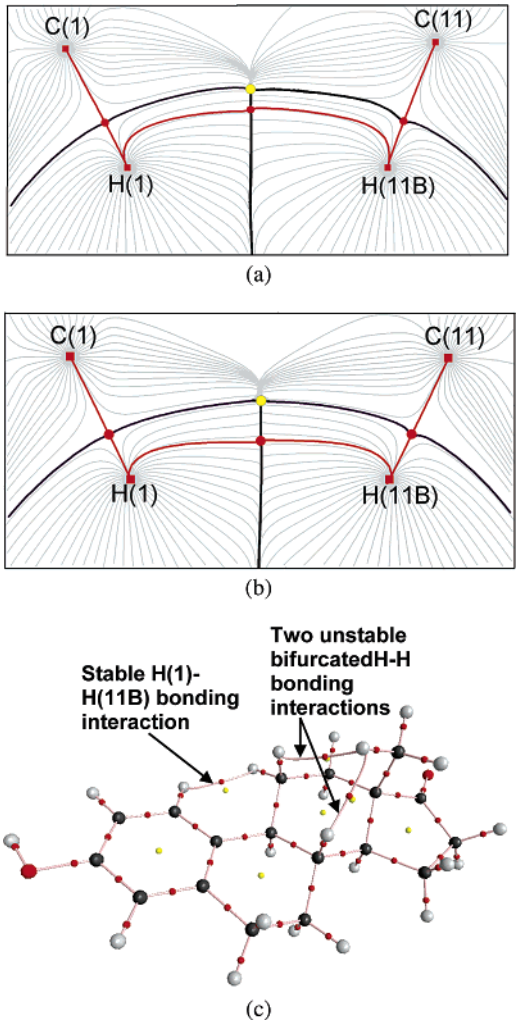

Figure 4. (a) The electron density gradient line map showing the H(1)—H(11B) interaction from the experimental data; (b) same from the theoretical solid-state data. The bond paths are shown as red lines, (3,−3) critical points are red squares, (3,−1) bond critical points are red circles, and (3,+1) ring critical points are yellow. (c) The molecular graph from the molecular theoretical calculation. Atoms are represented by colored balls: oxygens are red, carbons are black, and hydrogens are gray. The small red dots on the bond paths represent the bond critical points, and the yellow dots represent the ring critical points.

hydrogen atoms involved in H−H bonding are smaller in volume than corresponding atoms not involved in such bonding. A comparison of the volumes of H(1) with H(2) or H(4) reveals that H(1) is indeed the smallest in volume as revealed by experimental and theoretical values. Also, H(11B) is smaller in volume when compared to H(11A) [H(11A) is also involved in a H−H bonding interaction with H(18A), but the H(11A)−H(18A) interaction is topologically unstable and much weaker than the H(1)−H(11B) interaction (vide infra)].

Table 5 also lists the change in the energy of each atom in estrone with respect to the isolated elemental atomic ground state. From the table, we can see that H(1) is 87.5 kcal/mol more stable than atomic hydrogen (compared to only 84.4 and 79.1 kcal/mol for H(2) and H(4), respectively). In other words, H(1) is, on the average, ca. 5.8 kcal/mol more stable than the two other aromatic hydrogen atoms in estrone. The table also reveals that H(11B), which is involved in a relatively strong and topologically stable H−H bond to H(1), is significantly more stable than all other "regular" methylene hydrogen atoms in the saturated six-membered rings of estrone such as H(6 A or B), H(7 A or B), or H(12A or B) as can be gleaned from the table. The average relative energy of these six "regular" methylene hydrogen atoms is 90.4 kcal/mol with a standard deviation of 1.9 kcal/mol, i.e., H(11B) is ca. 4.8 kcal/mol more stable than an average methylene hydrogen. On the other hand, H(11B) is more stable than its geminal counterpart H(11A), which is not involved in H−H bonding, by 2.4 kcal/mol. Thus, a conservative estimate of the locally stabilizing contribution of the H(1)−H(11B) bonding interaction to the total molecular energy is ca. 8.2 kcal/mol when the energy of the H(11B) atom is gauged against its geminal H(11A) and this value rises to ca. 10.6 kcal/mol if it is gauged against the remaining "regular" methylene hydrogens in estrone. These findings are in complete agreement with similar H−H interactions previously reported.[65,66] It is emphasized that the local stabilization accompanying an H−H bonding interaction is *not* to be confused with a bond energy or a bond dissociation energy, which is impossible to define for this bonding interaction in this molecule. Also, the relative stabilization imparted by such bonding is often accompanied by the destabilization of other atoms in the molecule, a destabilization which can be dominant causing planar biphenyl to twist for example.[65,66] In estrone, the relative stability of the hydrogen atoms involved in the H(1)−H(11B) bonding interaction is accompanied by a relative destabilization of the carbon atoms directly bonded to them, C(1) and C(11), as well as the two carbon atoms linking rings **A** and **C**, namely, C(10) and C(9). As can be gleaned from Table 5, C(1) is the second least stable atom in ring **A** [following only C(3) which is bonded to the hydroxyl group]. Similarly, the table also shows that C(11) is the least stable in Ring **C**. Furthermore, a comparison of C(10) with C(5) shows that C(10) is relatively destabilized by 3 kcal/mol, while a comparison of C(9) with C(8) shows that C(9) is 15 kcal/mol less stable than C(8). Thus, the local stabilization gained due to the H−H bonding interaction appears to be at least offset if not overwhelmed by the relative destabilization of other parts of estrone, particularly carbon atoms C(1), C(10), C(9), and C(11).

The molecular graph of the gas-phase calculation reveals two additional H−H bonding interactions (three in total), (Figure 4c). The H(1)−H(11B) bond path is topologically stable being sufficiently distant from the associated ring critical point (0.384 Å) and is the one observed experimentally. The other two form a bifurcated system [H11(A)−H(18A)−H(8)] which is topologically unstable in view of the close proximity of the H−H bond critical points to their respective ring critical points (0.099 and 0.218 Å, respectively). Unlike the stable and persistent H(1)−H(11B) bond path, the H11(A)−H(18A) and H(18A)−H(8) bond paths could not be observed experimentally and both vanish with minor geometrical alterations or change in computational level (they disappear, for example, in the electron density calculated at the B3LYP/6-31G(d,p)//B3LYP/6-31G(d,p) level of theory).

From Table 5, one can see that the root-mean-square and the maximum integrated atomic Laplacian function are reasonably small for both experimental and calculated densities demonstrating the accuracy of the integrations. All the atomic charges sum to small nonzero values showing that the molecules are practically electroneutral as required. The sums of atomic volumes reproduce the unit cell volume per molecule with a

Table 5. Integrated Atomic Charges and Volumes[a,b]

atom	$q(\Omega)$, e$^-$ experiment, crystal	$q(\Omega)$, e$^-$ theory, crystal	$q(\Omega)$, e$^-$ theory, molecule	vol(Ω), Å^3 experiment, crystal	vol(Ω), Å^3 theory, crystal	vol(Ω), Å^3 theory, molecule	rel $E(\Omega)$,[c] kcal/mol theory, molecule
O(1)	−0.98	−1.04	−1.08	18.13	17.99	18.03	−539.6
O(2)	−1.17	−1.14	−1.10	18.82	18.10	20.61	−612.0
C(1)	0.05	−0.04	−0.02	12.51	12.93	12.04	−140.0
C(2)	0.00	−0.06	−0.04	12.31	12.68	12.63	−144.0
C(3)	0.40	0.35	0.48	8.79	9.01	9.10	+48.3
C(4)	0.12	−0.01	−0.02	11.36	11.83	12.29	−147.9
C(5)	0.03	−0.07	−0.01	10.14	10.13	10.31	−148.8
C(6)	0.17	0.03	0.05	8.19	8.59	8.52	−100.5
C(7)	0.05	0.03	0.05	7.77	8.06	8.37	−104.9
C(8)	0.04	0.04	0.05	6.62	6.63	6.66	−117.4
C(9)	0.03	0.02	0.05	6.93	7.01	6.91	−102.1
C(10)	−0.09	−0.05	−0.03	10.72	10.43	10.45	−145.8
C(11)	0.06	−0.01	0.05	7.83	7.97	8.06	−97.3
C(12)	0.01	0.02	0.05	8.01	8.11	8.13	−101.2
C(13)	0.04	0.03	0.02	6.16	6.12	6.24	−148.3
C(14)	−0.00	0.02	0.04	6.55	6.56	6.60	−137.8
C(15)	−0.02	0.000	0.04	8.68	8.32	8.53	−98.4
C(16)	−0.05	−0.06	−0.01	9.44	9.45	9.16	−124.3
C(17)	0.91	0.89	0.94	6.42	6.43	6.69	+270.0
C(18)	0.16	0.03	0.06	9.53	9.21	9.21	−96.8
H(1A)	0.54	0.58	0.55	1.99	1.95	3.48	+82.7
H(1)	0.00	0.06	0.01	6.68	6.42	6.91	−87.5
H(2)	0.01	0.06	0.00	6.77	6.91	7.50	−84.4
H(4)	0.00	0.07	0.03	8.14	7.51	7.27	−79.1
H(6a)	−0.03	0.01	−0.01	7.56	7.88	7.40	−89.2
H(6b)	−0.02	0.05	−0.00	7.38	7.39	7.38	−89.2
H(7a)	−0.05	−0.02	−0.02	6.80	7.13	7.38	−93.0
H(7b)	−0.05	0.02	−0.02	7.23	7.10	7.40	−92.1
H(8)	−0.01	0.01	−0.03	7.38	7.53	6.90	−98.3
H(9)	−0.01	0.02	−0.02	7.03	6.92	7.20	−96.4
H(11A)	0.00	−0.01	−0.02	7.84	7.96	7.13	−92.8
H(11B)	0.00	0.02	−0.02	6.93	6.91	6.98	−95.2
H(12A)	−0.06	0.04	0.00	7.46	7.51	7.37	−87.5
H(12B)	−0.06	0.01	−0.01	7.57	7.46	7.36	−91.2
H(14)	−0.02	0.00	−0.03	7.11	7.25	7.23	−101.0
H(15A)	0.03	0.00	−0.02	7.01	7.11	7.28	−92.2
H(15B)	0.02	0.02	−0.01	7.76	7.87	7.47	−90.1
H(16A)	−0.01	0.05	0.03	8.13	7.78	7.26	−79.7
H(16B)	−0.01	0.05	0.02	8.24	8.26	7.33	−79.5
H(18A)	−0.02	0.01	−0.02	8.03	8.04	6.42	−86.5
H(18B)	−0.02	−0.01	−0.00	6.31	6.08	7.22	−81.7
H(18C)	−0.01	0.00	−0.02	6.29	6.38	6.92	−87.8
Σ	0.02	0.03	0.01	350.56	350.91	353.31	-4580.7
L_{err}, au	0.0006	0.0006	0.0006				
L_{max}, au	0.0016	0.0015	0.0015				

[a] $L_{err} = (\Sigma L_\Omega^2/N_{atoms})^{1/2}$, $L_\Omega = -{}^1/_4(\nabla^2\rho)_\Omega$;[80] unit cell volume/4 = 351.95 Å^3. [b] The levels of theory used for the theoretical calculations are described in the "Experimental and Computational Details" section, but we emphasize here that the results reported in this table for the isolated molecule calculations are based on the B3LYP/6-311++G(d,p)//(experimental geometry) level of theory except the reported relative atomic energies which are based on fully optimized geometries at the B3LYP/6-31G(d,p) (see footnote (c)). [c] Relative energies (in kcal/mol) are calculated at the B3LYP/6-31G(d,p)//B3LYP/6-31G(d,p) level of theory with respect to the energies of the free ground-state elemental atoms which at the B3LYP/6-31G(d,p) level are: $E[H(^2S_{1/2})] = -0.500\,273$ au; $E[C(^3P_0)] = -37.846\,280$ au; and $E[O(^3P_2)] = -75.060\,623$ au. A negative entry means that the atom in estrone is more stable than that in the free atomic state.

maximum error of 0.4%, the volume of an individual estrone molecule ranging from ca. 351 Å^3 (experiment and periodic calculation) to ca. 353 Å^3 (gas-phase molecular calculation). There is a reasonable agreement between the "experimental" and "theoretical" charges, all being essentially zero except for atoms of the hydroxyl (C(3)−O(1)−H(1A)) and carbonyl (C(17)−O(2)) groups, as expected.[69] In the experimental case (but not in either periodic or molecular calculations), there are also significant charges on the C(4), C(6), and C(18) atoms, possibly due to the correlations between the multipole and thermal parameters, which were not completely eliminated.

The charge of −0.98 e on O(1) is gained almost completely at the expense of the populations of the atoms directly bonded to it, namely, H(1A) and C(3), which carry positive charges of 0.54 and 0.40 e, respectively. Similarly, the −1.17 e charge of O(2) comes almost entirely from C(17) to which it is bonded. These observations are reproduced by both the periodic and the molecular calculations.

Each oxygen atom is significantly more stable than its atomic ground-state O($^3P_2$), as can be seen from the values of the relative atomic energies listed in Table 5, a stabilization caused by this substantial gain in electronic population. In contrast, the atoms directly bonded to these oxygen atoms exhibit marked destabilization as they lose electronic charge to the oxygens.

(69) Anstead, G. M.; Carlson, K. E.; Katzenellenbogen, J. A. *Steroids* **1997**, *62*, 268−303.

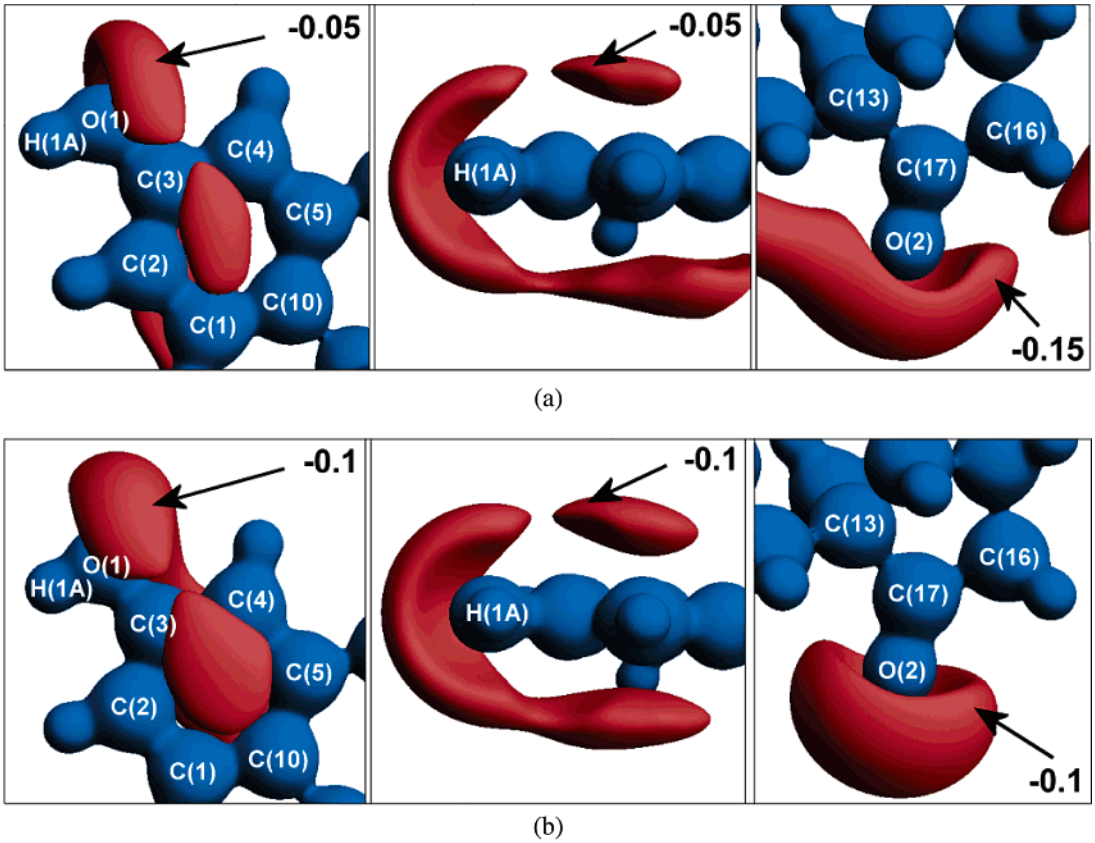

Figure 5. 3D-views of the electrostatic potential around the hydroxyl group and the aromatic ring (left and middle) and carbonyl group (right): (a) from the experimental data, (b) from the solid state theoretical data. Blue isosurfaces are 1.0 eÅ^{-1}; red isosurfaces are as those indicated on the pictures in eÅ^{-1}.

The three atoms bonded to the two oxygen atoms are the only atoms in estrone to be *destabilized* with respect to their free ground state, all remaining atoms in this molecule being significantly more stable than in its free ground state. The degree of destabilization of these three atoms parallel the amount of electron population lost to the adjacent oxygen. Thus, C(3) which loses 0.4 e is destabilized by only 48.3 kcal/mol, to be contrasted with C(17) which loses almost an entire electronic charge and, as a consequence, is destabilized by as much as 270.0 kcal/mol with respect to atomic C($^3P_0$). H(1A) is the only remaining atom to be destabilized (by 82.7 kcal/mol) with respect to its free ground state [H($^2S_{1/2}$)] due to the transfer of half of its electron population to its bonded oxygen O(1).

All atoms except H(1A), C(3), and C(17) are stabilized to different degrees in the molecule with respect to their free atomic states. The aromatic carbon atoms of estrone (except the carbon attached to the hydroxyl group, C(3)) are all significantly more stable than C($^3P_0$) by an average of 145.3(3.2) kcal/mol. The aliphatic carbon atoms of this molecule are also significantly more stable than C($^3P_0$), with no exceptions, by an average of 111.7(17.0) kcal/mol. The higher relative stability of an average aromatic carbon with respect to an average aliphatic carbon in estrone (ca. 34 kcal/mol difference) is clearly due to aromatic stabilization as expected.

Electrostatic Potential. The electrostatic potential (ESP) can be calculated directly from the electron density:

$$V(\mathbf{r}) = \sum_A \frac{Z_A}{|\mathbf{R}_A - \mathbf{r}|} - \int \frac{\rho(\mathbf{r}')}{|\mathbf{r}' - \mathbf{r}|} d\mathbf{r}' \qquad (5)$$

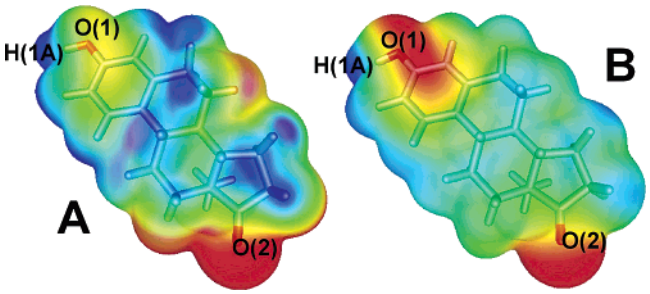

Figure 6. The electrostatic potential mapped on the molecular surface (ρ = 0.001 au = 0.006 75 eÅ^{-3}): (a) from the experimental data, (b) from the solid state theoretical data. Color scheme ranges from red (−0.1 eÅ^{-1}) via green (zero) to blue (0.1 eÅ^{-1}) (−32.2−32.2 kcal/(e mol)). The graphical program *gOpenMol*[81] was used to plot the data.

Z_A is the charge of nucleus A located at $\mathbf{R}_A$, and $\rho(\mathbf{r}')$ is the total electron density. Partition of the electron density into pseudoatomic fragments in the form of a multipole expansion allows the direct space calculation of the ESP distribution.[70] 3D-ESP distributions calculated for a single molecule in the solid state are shown in Figure 5. The ESP mapped on the molecular surface, defined as the electron density isosurface of 0.001 au,[71,41] for a single molecule taken from the solid state is shown in Figure 6. The molecular volume within this ρ = 0.001 au surface is ca. 330 Å^3 (~20 Å^3 less than the total ascribed volume delimited by the sum of atomic zero-flux surfaces), which easily fits the estrogen receptor probe accessible volume

(70) Su, Z.; Coppens, P. *Acta Crystallogr.* **1992**, *A48*, 188−197.
(71) Bader, R. F. W.; Carroll, M. T.; Cheeseman, J. R.; Chang, C. *J. Am. Chem. Soc.* **1987**, *109*, 7968−7979.

of ca. 450 Å^3.[72] There is a quantitative difference between the experimental and theoretical ESP distributions, but qualitatively they are the same: there are significant negative areas around the hydroxyl and carbonyl groups.[73] The negative area around the O(1) atom is much more localized compared with the extensive area around the carbonyl group, especially in the experimental case. There are also considerable negative regions above and below the aromatic ring, where the π-electrons are expected to be. This ESP distribution is in excellent agreement with the earlier theoretically calculated electrostatic potential pattern for the estrone molecule.[74] When the hydrogen bond is formed in the estrone crystal, the positive ESP area around the H(1A) atom is electrostatically attracted by the highly negative area around the O(2) atom. These negative ESP areas can be considered as possible locations of initial ligand−receptor electrostatic interactions when the estrogen receptor and a ligand start to "see" each other.[75,76] ER-ligand final binding takes place through both hydrogen bonding and van der Waals interactions.[77] As has been shown by Anstead et al.,[69] the phenolic OH group in the **A**-ring (Figure 1a) of the *estradiol* molecule[78] contributes ∼1.9 kcal/mol to the binding free energy, and the aromatic ring contributes ∼1.5 kcal/mol to the total of 12 kcal/mol. The hydroxyl group is assumed to act as a hydrogen bond donor, and the aromatic ring is supposed to have "weak polar interactions" with receptor residues.[69] Both the hydroxyl group and the aromatic ring[79] have significant negative ESP areas in the estrone molecule as well as in estradiol[38] which provide at least the initial driving force toward binding of these areas. The high positive charge of H(1A) and the highly negative charges of both oxygen atoms (Table 5) of the estrone molecule should provide strong hydrogen bonding to the estrogen receptor.

Conclusions

This paper reports the first accurately determined topological properties of the electron density and the electrostatic potential of the hormone molecule estrone. Significant ESP negative areas around the hydroxyl and carbonyl groups have been found both experimentally and theoretically. The negative area associated with the hydroxyl group is much more localized compared with the extensive area around the carbonyl group. Considerable negative regions above and below the aromatic ring, where the π-electrons are expected to be, are also observed. These negative ESP areas are the possible locations of *initial* ligand−receptor electrostatic interactions, with the hydroxyl group being assumed to act as a hydrogen bond donor and the aromatic ring being supposed to have "weak polar interactions" with receptor residues. The observed high positive charge of hydroxyl hydrogen and the highly negative charges of both oxygen atoms of the estrone molecule ensure strong hydrogen bonding to the estrogen receptor.

An excellent agreement was found between the experimental bond and atomic properties and those calculated from periodic and isolated molecular calculations. The agreement between calculated and experimental one-electron properties encouraged us to explore the possibility of empirically correlating the carbon−carbon delocalization indices (which require the full density matrix for their evaluation, information which is not normally available from experiment) with the experimental electron density at the bond critical point. The excellent statistics of the fit between the electron density at the bond critical point and the delocalization indices between bonded carbon atoms (a measure of the bond order between them) promises that such empirical correlations may be used in the future to obtain information on electron-pair sharing empirically from experiment.

An analysis of the atomic energies of the atoms in estrone reveals that all atoms are more stable than their respective isolated atomic ground states with the exception of three atoms which were found to be less stable than in their isolated state. These are the atoms directly bonded to the two oxygen atoms, namely, the phenolic C(3), the phenolic H(1A), and the carbonyl C(17). The destabilization of these three atoms is brought about by the significant transfer of their electron population to the more electronegative neighboring oxygen atom.

The estrone molecule exhibits a stable hydrogen−hydrogen bond path linking the nuclei of H(1) and H(11B) in experimentally and theoretically calculated densities. The analysis of atomic energies reveals that this H−H closed-shell bonding interaction is accompanied with an estimated local stabilization of 8−11 kcal/mol.

Acknowledgment. We would like to thank Dr. S. Brooks for his insight and encouragement to begin this study. We also thank Dr. A. Stash and Prof. V. Tsirelson for making the programs *WinXPRO* and *XDRKplot* available for us and for the valuable discussions. We appreciate the assistance of Dr. J. Overgaard in plotting of the ESP pictures on molecular surfaces. We acknowledge the financial support of the Killam Trusts to one of us (C.F.M.) in the form of an I. W. Killam Postdoctoral Fellowship. We thank the Department of Defense, USAMRMC, for financial support, Grant Number DAMD17-99-1-9408.

Supporting Information Available: Experimental reflection statistics, atomic coordinates, thermal and multipole parameters, interatomic distances and angles, electrostatic potential maps, molecular optimized geometry, vibrational frequencies and Gaussian archival output. This material is available free of charge via the Internet at http://pubs.acs.org.

JA061080V

(72) Brzozowski, A. M.; Pike, A. C. W.; Dauter, Z.; Hubbard, R. E.; Bonn, T.; Engström, O.; Öhman, L.; Greene, G. L.; Gustafsson, J.-Å.; Carlquist, M. *Nature* **1997**, *389*, 753−758.
(73) In the experimental case, there is also a negative area around the H(9) atom, which carries a slightly negative atomic charge (Table 6).
(74) Kubli-Garfias, C. *THEOCHEM* **1998**, *452*, 175−183.
(75) Politzer, P.; Murray, J. S.; Peralta-Inga, Z. *Int. J. Quantum Chem.* **2001**, *85*, 676−684.
(76) Politzer, P.; Murray, J. S. *Theor. Chem. Acc.* **2002**, *108*, 134−142.
(77) Hu, J.-Y.; Aizawa, T. *Water Res.* **2003**, *37*, 1213−1222.
(78) The estradiol molecule has another hydroxyl group in the 17-position.
(79) As well as the carbonyl group, which probably acts as a hydrogen bond acceptor.
(80) Flensburg, C.; Madsen, D. *Acta Crystallogr.* **2000**, *A56*, 24−28.
(81) The *gOpenMol* program (www.csc.fi/gopenmol).